BABAR-CONF-05/018
SLAC-PUB-11377
July 2005

Measurement of γ in $B^{\mp} \to D^{(*)}K^{\mp}$ and $B^{\mp} \to DK^{*\mp}$ decays with a Dalitz analysis of $D \to K^0_S\pi^-\pi^+$

The *BABAR* Collaboration

February 7, 2008

Abstract

We present a measurement of the Cabibbo-Kobayashi-Maskawa *CP*-violating phase γ with a Dalitz plot analysis of neutral D-meson decays to the $K^0_S\pi^-\pi^+$ final state from $B^{\mp} \to D^{(*)}K^{\mp}$ and $B^{\mp} \to DK^{*\mp}$ decays, using a sample of 227 million $B\overline{B}$ pairs collected by the *BABAR* detector. We measure $\gamma = (67 \pm 28 \pm 13 \pm 11)^{\circ}$, where the first error is statistical, the second is the experimental systematic uncertainty and the third reflects the Dalitz model uncertainty. This result suffers from a two-fold ambiguity. The contribution to the Dalitz model uncertainty due to the description of the $\pi\pi$ S-wave in $D^0 \to K^0_S\pi^-\pi^+$, evaluated using a K-matrix formalism, is found to be 3°.

Submitted at the International Europhysics Conference On High-Energy Physics (HEP 2005), 7/21—7/27/2005, Lisbon, Portugal

Stanford Linear Accelerator Center, Stanford University, Stanford, CA 94309

Work supported in part by Department of Energy contract DE-AC03-76SF00515.

The *BABAR* Collaboration,

B. Aubert, R. Barate, D. Boutigny, F. Couderc, Y. Karyotakis, J. P. Lees, V. Poireau, V. Tisserand, A. Zghiche

Laboratoire de Physique des Particules, F-74941 Annecy-le-Vieux, France

E. Grauges

IFAE, Universitat Autonoma de Barcelona, E-08193 Bellaterra, Barcelona, Spain

A. Palano, M. Pappagallo, A. Pompili

Università di Bari, Dipartimento di Fisica and INFN, I-70126 Bari, Italy

J. C. Chen, N. D. Qi, G. Rong, P. Wang, Y. S. Zhu

Institute of High Energy Physics, Beijing 100039, China

G. Eigen, I. Ofte, B. Stugu

University of Bergen, Institute of Physics, N-5007 Bergen, Norway

G. S. Abrams, M. Battaglia, A. B. Breon, D. N. Brown, J. Button-Shafer, R. N. Cahn, E. Charles, C. T. Day, M. S. Gill, A. V. Gritsan, Y. Groysman, R. G. Jacobsen, R. W. Kadel, J. Kadyk, L. T. Kerth, Yu. G. Kolomensky, G. Kukartsev, G. Lynch, L. M. Mir, P. J. Oddone, T. J. Orimoto, M. Pripstein, N. A. Roe, M. T. Ronan, W. A. Wenzel

Lawrence Berkeley National Laboratory and University of California, Berkeley, California 94720, USA

M. Barrett, K. E. Ford, T. J. Harrison, A. J. Hart, C. M. Hawkes, S. E. Morgan, A. T. Watson

University of Birmingham, Birmingham, B15 2TT, United Kingdom

M. Fritsch, K. Goetzen, T. Held, H. Koch, B. Lewandowski, M. Pelizaeus, K. Peters, T. Schroeder, M. Steinke

Ruhr Universität Bochum, Institut für Experimentalphysik 1, D-44780 Bochum, Germany

J. T. Boyd, J. P. Burke, N. Chevalier, W. N. Cottingham

University of Bristol, Bristol BS8 1TL, United Kingdom

T. Cuhadar-Donszelmann, B. G. Fulsom, C. Hearty, N. S. Knecht, T. S. Mattison, J. A. McKenna

University of British Columbia, Vancouver, British Columbia, Canada V6T 1Z1

A. Khan, P. Kyberd, M. Saleem, L. Teodorescu

Brunel University, Uxbridge, Middlesex UB8 3PH, United Kingdom

A. E. Blinov, V. E. Blinov, A. D. Bukin, V. P. Druzhinin, V. B. Golubev, E. A. Kravchenko, A. P. Onuchin, S. I. Serednyakov, Yu. I. Skovpen, E. P. Solodov, A. N. Yushkov

Budker Institute of Nuclear Physics, Novosibirsk 630090, Russia

D. Best, M. Bondioli, M. Bruinsma, M. Chao, S. Curry, I. Eschrich, D. Kirkby, A. J. Lankford, P. Lund, M. Mandelkern, R. K. Mommsen, W. Roethel, D. P. Stoker

University of California at Irvine, Irvine, California 92697, USA

C. Buchanan, B. L. Hartfiel, A. J. R. Weinstein

University of California at Los Angeles, Los Angeles, California 90024, USA

S. D. Foulkes, J. W. Gary, O. Long, B. C. Shen, K. Wang, L. Zhang

University of California at Riverside, Riverside, California 92521, USA

D. del Re, H. K. Hadavand, E. J. Hill, D. B. MacFarlane, H. P. Paar, S. Rahatlou, V. Sharma

University of California at San Diego, La Jolla, California 92093, USA

J. W. Berryhill, C. Campagnari, A. Cunha, B. Dahmes, T. M. Hong, M. A. Mazur, J. D. Richman, W. Verkerke

University of California at Santa Barbara, Santa Barbara, California 93106, USA

T. W. Beck, A. M. Eisner, C. J. Flacco, C. A. Heusch, J. Kroseberg, W. S. Lockman, G. Nesom, T. Schalk, B. A. Schumm, A. Seiden, P. Spradlin, D. C. Williams, M. G. Wilson

University of California at Santa Cruz, Institute for Particle Physics, Santa Cruz, California 95064, USA

J. Albert, E. Chen, G. P. Dubois-Felsmann, A. Dvoretskii, D. G. Hitlin, I. Narsky, T. Piatenko, F. C. Porter, A. Ryd, A. Samuel

California Institute of Technology, Pasadena, California 91125, USA

R. Andreassen, S. Jayatilleke, G. Mancinelli, B. T. Meadows, M. D. Sokoloff

University of Cincinnati, Cincinnati, Ohio 45221, USA

F. Blanc, P. Bloom, S. Chen, W. T. Ford, J. F. Hirschauer, A. Kreisel, U. Nauenberg, A. Olivas, P. Rankin, W. O. Ruddick, J. G. Smith, K. A. Ulmer, S. R. Wagner, J. Zhang

University of Colorado, Boulder, Colorado 80309, USA

A. Chen, E. A. Eckhart, J. L. Harton, A. Soffer, W. H. Toki, R. J. Wilson, Q. Zeng

Colorado State University, Fort Collins, Colorado 80523, USA

D. Altenburg, E. Feltresi, A. Hauke, B. Spaan

Universität Dortmund, Institut fur Physik, D-44221 Dortmund, Germany

T. Brandt, J. Brose, M. Dickopp, V. Klose, H. M. Lacker, R. Nogowski, S. Otto, A. Petzold, G. Schott, J. Schubert, K. R. Schubert, R. Schwierz, J. E. Sundermann

Technische Universität Dresden, Institut für Kern- und Teilchenphysik, D-01062 Dresden, Germany

D. Bernard, G. R. Bonneaud, P. Grenier, S. Schrenk, Ch. Thiebaux, G. Vasileiadis, M. Verderi

Ecole Polytechnique, LLR, F-91128 Palaiseau, France

D. J. Bard, P. J. Clark, W. Gradl, F. Muheim, S. Playfer, Y. Xie

University of Edinburgh, Edinburgh EH9 3JZ, United Kingdom

M. Andreotti, V. Azzolini, D. Bettoni, C. Bozzi, R. Calabrese, G. Cibinetto, E. Luppi, M. Negrini, L. Piemontese

Università di Ferrara, Dipartimento di Fisica and INFN, I-44100 Ferrara, Italy

F. Anulli, R. Baldini-Ferroli, A. Calcaterra, R. de Sangro, G. Finocchiaro, P. Patteri, I. M. Peruzzi,[1] M. Piccolo, A. Zallo

Laboratori Nazionali di Frascati dell'INFN, I-00044 Frascati, Italy

[1]Also with Università di Perugia, Dipartimento di Fisica, Perugia, Italy

A. Buzzo, R. Capra, R. Contri, M. Lo Vetere, M. Macri, M. R. Monge, S. Passaggio, C. Patrignani, E. Robutti, A. Santroni, S. Tosi

Università di Genova, Dipartimento di Fisica and INFN, I-16146 Genova, Italy

G. Brandenburg, K. S. Chaisanguanthum, M. Morii, E. Won, J. Wu

Harvard University, Cambridge, Massachusetts 02138, USA

R. S. Dubitzky, U. Langenegger, J. Marks, S. Schenk, U. Uwer

Universität Heidelberg, Physikalisches Institut, Philosophenweg 12, D-69120 Heidelberg, Germany

W. Bhimji, D. A. Bowerman, P. D. Dauncey, U. Egede, R. L. Flack, J. R. Gaillard, G. W. Morton, J. A. Nash, M. B. Nikolich, G. P. Taylor, W. P. Vazquez

Imperial College London, London, SW7 2AZ, United Kingdom

M. J. Charles, W. F. Mader, U. Mallik, A. K. Mohapatra

University of Iowa, Iowa City, Iowa 52242, USA

J. Cochran, H. B. Crawley, V. Eyges, W. T. Meyer, S. Prell, E. I. Rosenberg, A. E. Rubin, J. Yi

Iowa State University, Ames, Iowa 50011-3160, USA

N. Arnaud, M. Davier, X. Giroux, G. Grosdidier, A. Höcker, F. Le Diberder, V. Lepeltier, A. M. Lutz, A. Oyanguren, T. C. Petersen, M. Pierini, S. Plaszczynski, S. Rodier, P. Roudeau, M. H. Schune, A. Stocchi, G. Wormser

Laboratoire de l'Accélérateur Linéaire, F-91898 Orsay, France

C. H. Cheng, D. J. Lange, M. C. Simani, D. M. Wright

Lawrence Livermore National Laboratory, Livermore, California 94550, USA

A. J. Bevan, C. A. Chavez, I. J. Forster, J. R. Fry, E. Gabathuler, R. Gamet, K. A. George, D. E. Hutchcroft, R. J. Parry, D. J. Payne, K. C. Schofield, C. Touramanis

University of Liverpool, Liverpool L69 72E, United Kingdom

C. M. Cormack, F. Di Lodovico, W. Menges, R. Sacco

Queen Mary, University of London, E1 4NS, United Kingdom

C. L. Brown, G. Cowan, H. U. Flaecher, M. G. Green, D. A. Hopkins, P. S. Jackson, T. R. McMahon, S. Ricciardi, F. Salvatore

University of London, Royal Holloway and Bedford New College, Egham, Surrey TW20 0EX, United Kingdom

D. Brown, C. L. Davis

University of Louisville, Louisville, Kentucky 40292, USA

J. Allison, N. R. Barlow, R. J. Barlow, C. L. Edgar, M. C. Hodgkinson, M. P. Kelly, G. D. Lafferty, M. T. Naisbit, J. C. Williams

University of Manchester, Manchester M13 9PL, United Kingdom

C. Chen, W. D. Hulsbergen, A. Jawahery, D. Kovalskyi, C. K. Lae, D. A. Roberts, G. Simi

University of Maryland, College Park, Maryland 20742, USA

G. Blaylock, C. Dallapiccola, S. S. Hertzbach, R. Kofler, V. B. Koptchev, X. Li, T. B. Moore, S. Saremi, H. Staengle, S. Willocq

University of Massachusetts, Amherst, Massachusetts 01003, USA

R. Cowan, K. Koeneke, G. Sciolla, S. J. Sekula, M. Spitznagel, F. Taylor, R. K. Yamamoto

Massachusetts Institute of Technology, Laboratory for Nuclear Science, Cambridge, Massachusetts 02139, USA

H. Kim, P. M. Patel, S. H. Robertson

McGill University, Montréal, Quebec, Canada H3A 2T8

A. Lazzaro, V. Lombardo, F. Palombo

Università di Milano, Dipartimento di Fisica and INFN, I-20133 Milano, Italy

J. M. Bauer, L. Cremaldi, V. Eschenburg, R. Godang, R. Kroeger, J. Reidy, D. A. Sanders, D. J. Summers, H. W. Zhao

University of Mississippi, University, Mississippi 38677, USA

S. Brunet, D. Côté, P. Taras, B. Viaud

Université de Montréal, Laboratoire René J. A. Lévesque, Montréal, Quebec, Canada H3C 3J7

H. Nicholson

Mount Holyoke College, South Hadley, Massachusetts 01075, USA

N. Cavallo,[2] G. De Nardo, F. Fabozzi,[2] C. Gatto, L. Lista, D. Monorchio, P. Paolucci, D. Piccolo, C. Sciacca

Università di Napoli Federico II, Dipartimento di Scienze Fisiche and INFN, I-80126, Napoli, Italy

M. Baak, H. Bulten, G. Raven, H. L. Snoek, L. Wilden

NIKHEF, National Institute for Nuclear Physics and High Energy Physics, NL-1009 DB Amsterdam, The Netherlands

C. P. Jessop, J. M. LoSecco

University of Notre Dame, Notre Dame, Indiana 46556, USA

T. Allmendinger, G. Benelli, K. K. Gan, K. Honscheid, D. Hufnagel, P. D. Jackson, H. Kagan, R. Kass, T. Pulliam, A. M. Rahimi, R. Ter-Antonyan, Q. K. Wong

Ohio State University, Columbus, Ohio 43210, USA

J. Brau, R. Frey, O. Igonkina, M. Lu, C. T. Potter, N. B. Sinev, D. Strom, J. Strube, E. Torrence

University of Oregon, Eugene, Oregon 97403, USA

F. Galeazzi, M. Margoni, M. Morandin, M. Posocco, M. Rotondo, F. Simonetto, R. Stroili, C. Voci

Università di Padova, Dipartimento di Fisica and INFN, I-35131 Padova, Italy

M. Benayoun, H. Briand, J. Chauveau, P. David, L. Del Buono, Ch. de la Vaissière, O. Hamon, M. J. J. John, Ph. Leruste, J. Malclès, J. Ocariz, L. Roos, G. Therin

Universités Paris VI et VII, Laboratoire de Physique Nucléaire et de Hautes Energies, F-75252 Paris, France

[2]Also with Università della Basilicata, Potenza, Italy

P. K. Behera, L. Gladney, Q. H. Guo, J. Panetta
University of Pennsylvania, Philadelphia, Pennsylvania 19104, USA

M. Biasini, R. Covarelli, S. Pacetti, M. Pioppi
Università di Perugia, Dipartimento di Fisica and INFN, I-06100 Perugia, Italy

C. Angelini, G. Batignani, S. Bettarini, F. Bucci, G. Calderini, M. Carpinelli, R. Cenci, F. Forti, M. A. Giorgi, A. Lusiani, G. Marchiori, M. Morganti, N. Neri, E. Paoloni, M. Rama, G. Rizzo, J. Walsh
Università di Pisa, Dipartimento di Fisica, Scuola Normale Superiore and INFN, I-56127 Pisa, Italy

M. Haire, D. Judd, D. E. Wagoner
Prairie View A&M University, Prairie View, Texas 77446, USA

J. Biesiada, N. Danielson, P. Elmer, Y. P. Lau, C. Lu, J. Olsen, A. J. S. Smith, A. V. Telnov
Princeton University, Princeton, New Jersey 08544, USA

F. Bellini, G. Cavoto, A. D'Orazio, E. Di Marco, R. Faccini, F. Ferrarotto, F. Ferroni, M. Gaspero, L. Li Gioi, M. A. Mazzoni, S. Morganti, G. Piredda, F. Polci, F. Safai Tehrani, C. Voena
Università di Roma La Sapienza, Dipartimento di Fisica and INFN, I-00185 Roma, Italy

H. Schröder, G. Wagner, R. Waldi
Universität Rostock, D-18051 Rostock, Germany

T. Adye, N. De Groot, B. Franek, G. P. Gopal, E. O. Olaiya, F. F. Wilson
Rutherford Appleton Laboratory, Chilton, Didcot, Oxon, OX11 0QX, United Kingdom

R. Aleksan, S. Emery, A. Gaidot, S. F. Ganzhur, P.-F. Giraud, G. Graziani, G. Hamel de Monchenault, W. Kozanecki, M. Legendre, G. W. London, B. Mayer, G. Vasseur, Ch. Yèche, M. Zito
DSM/Dapnia, CEA/Saclay, F-91191 Gif-sur-Yvette, France

M. V. Purohit, A. W. Weidemann, J. R. Wilson, F. X. Yumiceva
University of South Carolina, Columbia, South Carolina 29208, USA

T. Abe, M. T. Allen, D. Aston, N. van Bakel, R. Bartoldus, N. Berger, A. M. Boyarski, O. L. Buchmueller, R. Claus, J. P. Coleman, M. R. Convery, M. Cristinziani, J. C. Dingfelder, D. Dong, J. Dorfan, D. Dujmic, W. Dunwoodie, S. Fan, R. C. Field, T. Glanzman, S. J. Gowdy, T. Hadig, V. Halyo, C. Hast, T. Hryn'ova, W. R. Innes, M. H. Kelsey, P. Kim, M. L. Kocian, D. W. G. S. Leith, J. Libby, S. Luitz, V. Luth, H. L. Lynch, H. Marsiske, R. Messner, D. R. Muller, C. P. O'Grady, V. E. Ozcan, A. Perazzo, M. Perl, B. N. Ratcliff, A. Roodman, A. A. Salnikov, R. H. Schindler, J. Schwiening, A. Snyder, J. Stelzer, D. Su, M. K. Sullivan, K. Suzuki, S. Swain, J. M. Thompson, J. Va'vra, M. Weaver, W. J. Wisniewski, M. Wittgen, D. H. Wright, A. K. Yarritu, K. Yi, C. C. Young
Stanford Linear Accelerator Center, Stanford, California 94309, USA

P. R. Burchat, A. J. Edwards, S. A. Majewski, B. A. Petersen, C. Roat
Stanford University, Stanford, California 94305-4060, USA

M. Ahmed, S. Ahmed, M. S. Alam, J. A. Ernst, M. A. Saeed, F. R. Wappler, S. B. Zain
State University of New York, Albany, New York 12222, USA

W. Bugg, M. Krishnamurthy, S. M. Spanier
University of Tennessee, Knoxville, Tennessee 37996, USA

R. Eckmann, J. L. Ritchie, A. Satpathy, R. F. Schwitters

University of Texas at Austin, Austin, Texas 78712, USA

J. M. Izen, I. Kitayama, X. C. Lou, S. Ye

University of Texas at Dallas, Richardson, Texas 75083, USA

F. Bianchi, M. Bona, F. Gallo, D. Gamba

Università di Torino, Dipartimento di Fisica Sperimentale and INFN, I-10125 Torino, Italy

M. Bomben, L. Bosisio, C. Cartaro, F. Cossutti, G. Della Ricca, S. Dittongo, S. Grancagnolo, L. Lanceri, L. Vitale

Università di Trieste, Dipartimento di Fisica and INFN, I-34127 Trieste, Italy

F. Martinez-Vidal

IFIC, Universitat de Valencia-CSIC, E-46071 Valencia, Spain

R. S. Panvini[3]

Vanderbilt University, Nashville, Tennessee 37235, USA

Sw. Banerjee, B. Bhuyan, C. M. Brown, D. Fortin, K. Hamano, R. Kowalewski, J. M. Roney, R. J. Sobie

University of Victoria, Victoria, British Columbia, Canada V8W 3P6

J. J. Back, P. F. Harrison, T. E. Latham, G. B. Mohanty

Department of Physics, University of Warwick, Coventry CV4 7AL, United Kingdom

H. R. Band, X. Chen, B. Cheng, S. Dasu, M. Datta, A. M. Eichenbaum, K. T. Flood, M. Graham, J. J. Hollar, J. R. Johnson, P. E. Kutter, H. Li, R. Liu, B. Mellado, A. Mihalyi, Y. Pan, R. Prepost, P. Tan, J. H. von Wimmersperg-Toeller, S. L. Wu, Z. Yu

University of Wisconsin, Madison, Wisconsin 53706, USA

H. Neal

Yale University, New Haven, Connecticut 06511, USA

[3]Deceased

1 INTRODUCTION

CP violation in the Standard Model is described by a single phase in the Cabibbo-Kobayashi-Maskawa (CKM) quark-mixing matrix [1]. Although *CP* violation in the B system is now well established, further measurements of *CP* violation are needed to overconstrain the Unitarity Triangle [2] and confirm the CKM model or observe deviations from its predictions. The angle γ of the Unitarity Triangle is defined as $\gamma \equiv \arg\left[-V_{ud}V_{ub}^*/V_{cd}V_{cb}^*\right]$. Various methods [3, 4] have been proposed to extract γ using $B^- \to \tilde{D}^0 K^-$ [4] decays, all exploiting the interference between the color allowed $B^- \to D^0 K^-$ ($\propto V_{cb}$) and the color suppressed $B^- \to \overline{D}^0 K^-$ ($\propto V_{ub}$) transitions, when the D^0 and $\overline{D}^0$ are reconstructed in a common final state. The symbol $\tilde{D}^0$ indicates either a D^0 or a $\overline{D}^0$ meson. The extraction of γ with these decays is theoretically clean because the main contributions to the amplitudes come from tree-level transitions.

Among the $\tilde{D}^0$ decay modes studied so far the $K^0_S\pi^-\pi^+$ channel is the one with the highest sensitivity to γ because of the best overall combination of branching ratio magnitude, $D^0 - \overline{D}^0$ interference and background level. Both *BABAR* [5] and Belle [6] have reported on a measurement of γ based on $B^- \to \tilde{D}^{(*)0}K^-$ decays with a Dalitz analysis of $\tilde{D}^0 \to K^0_S\pi^-\pi^+$. Here, the symbol "$(*)$" refers to either a D or D^* meson. Belle has recently shown a preliminary result using $B^- \to \tilde{D}^0 K^{*-}$, $K^{*-} \to K^0_S\pi^-$ [7]. In this paper we report on the update of the γ measurement with the addition of the $B^- \to \tilde{D}^0 K^{*-}$, $K^{*-} \to K^0_S\pi^-$ decay mode to the previously used $B^- \to \tilde{D}^{(*)0}K^-$ channels.

Assuming no *CP* asymmetry in D decays and neglecting the $B^\mp \to \tilde{D}^0(K^0_S\pi^\mp)_{\mathrm{non}-K^*}$ contribution, the $B^\mp \to \tilde{D}^0 K^{*\mp}$, $\tilde{D}^0 \to K^0_S\pi^-\pi^+$, $K^{*\mp} \to K^0_S\pi^\mp$ decay chain rate $\Gamma_\mp(m^2_-, m^2_+)$ can be written as

$$\Gamma_\mp(m^2_-, m^2_+) \propto |\mathcal{A}_{D\mp}|^2 + r_B^2|\mathcal{A}_{D\pm}|^2 + 2\left\{x_\mp \,\mathrm{Re}[\mathcal{A}_{D\mp}\mathcal{A}^*_{D\pm}] + y_\mp \,\mathrm{Im}[\mathcal{A}_{D\mp}\mathcal{A}^*_{D\pm}]\right\} \ , \qquad (1)$$

where m^2_- and m^2_+ are the squared invariant masses of the $K^0_S\pi^-$ and $K^0_S\pi^+$ combinations respectively from the $\tilde{D}^0$ decay, and $\mathcal{A}_{D\mp} \equiv \mathcal{A}_D(m^2_\mp, m^2_\pm)$, with $\mathcal{A}_{D-}$ ($\mathcal{A}_{D+}$) the amplitude of the $D^0 \to K^0_S\pi^-\pi^+$ ($\overline{D}^0 \to K^0_S\pi^+\pi^-$) decay. In Eq. (1) we have introduced the *Cartesian coordinates* $x_\mp = r_B\cos(\delta_B \mp \gamma)$ and $y_\mp = r_B\sin(\delta_B \mp \gamma)$ [5], for which the constraint $r_B^2 = x_\mp^2 + y_\mp^2$ holds. Here, r_B is the magnitude of the ratio of the amplitudes $\mathcal{A}(B^- \to \overline{D}^0 K^{*-})$ and $\mathcal{A}(B^- \to D^0 K^{*-})$ and δ_B is their relative strong phase.

In the case where a $B^\mp \to \tilde{D}^0(K^0_S\pi^\mp)_{\mathrm{non}-K^*}$ component interferes with $B^\mp \to \tilde{D}^0 K^{*\mp}$, we write a general parameterization of the decay rates following the approach proposed in Ref. [8],

$$\Gamma_\mp(m^2_-, m^2_+) \propto |\mathcal{A}_{D\mp}|^2 + r_s^2|\mathcal{A}_{D\pm}|^2 + 2\left\{x_{s\mp} \,\mathrm{Re}[\mathcal{A}_{D\mp}\mathcal{A}^*_{D\pm}] + y_{s\mp} \,\mathrm{Im}[\mathcal{A}_{D\mp}\mathcal{A}^*_{D\pm}]\right\} \ , \qquad (2)$$

where $x_{s\mp} = \kappa r_s\cos(\delta_s \mp \gamma)$, $y_{s\mp} = \kappa r_s\sin(\delta_s \mp \gamma)$ and $x^2_{s\mp} + y^2_{s\mp} = \kappa^2 r_s^2$, with $0 \le \kappa \le 1$. In the limit of a null $B^\mp \to \tilde{D}^0(K^0_S\pi^\mp)_{\mathrm{non}-K^*}$ contribution, $\kappa \to 1$, $r_s \to r_B$ and $\delta_s \to \delta_B$. The parameterization given by Eq. (2) is also valid in the case when r_B and δ_B happen to vary within the K^* mass window, and accounts for efficiency variations as a function of the kinematics of the B decay.

Once the decay amplitude $\mathcal{A}_D$ is known, the Dalitz plot distributions for $\tilde{D}^0$ from B^- and B^+ decays can be simultaneously fitted to $\Gamma_-(m^2_-, m^2_+)$ and $\Gamma_+(m^2_-, m^2_+)$ as given by Eq. (2), respectively. A maximum likelihood technique can be used to estimate the *CP*-violating parameters $x_{s\mp}$, $y_{s\mp}$, and r_s^2. Since the parameter r_s^2 is also floated our $(x_{s\mp}, y_{s\mp})$ results do not depend on any assumption on the amount and nature of the $B^- \to \tilde{D}^0(K^0_S\pi^-)_{\mathrm{non}-K^*}$ component, while on

[4] Reference to the charge-conjugate state is implied here and throughout the text unless otherwise specified.

average the statistical uncertainties do not increase. Moreover, this general treatment allows us to consider the $B^- \to \tilde{D}^0(K^0_S\pi^-)_{\mathrm{non}-K^*}$ events like $B^- \to \tilde{D}^0 K^{*-}$ signal.

Since the measurement of γ arises from the interference term in Eq. (2), the uncertainty in the knowledge of the complex form of $\mathcal{A}_D$ can lead to a systematic uncertainty. Two different models describing the $D^0 \to K^0_S\pi^-\pi^+$ decay have been used in this analysis. The first model (also referred to as Breit-Wigner model) [9] is the same as used for our previously reported measurement of γ on $B^- \to \tilde{D}^{(*)0}K^-$, $\tilde{D}^0 \to K^0_S\pi^-\pi^+$ decays [5], and expresses $\mathcal{A}_D$ as a sum of two-body decay-matrix elements and a non-resonant contribution. In the second model (hereafter referred to as the $\pi\pi$ S-wave K-matrix model) the treatment of the $\pi\pi$ S-wave states in $D^0 \to K^0_S\pi^-\pi^+$ uses a K-matrix formalism [10, 11] to account for the non-trivial dynamics due to the presence of broad and overlapping resonances. The two models have been obtained using a high statistics flavor tagged D^0 sample ($D^{*+} \to D^0\pi^+_s$) selected from $e^+e^- \to c\bar{c}$ events recorded by *BABAR*.

2 THE *BABAR* DETECTOR AND DATASET

The analysis is based on a sample of 227 million $B\bar{B}$ pairs collected by the *BABAR* detector at the SLAC PEP-II e^+e^- asymmetric-energy storage ring. *BABAR* is a solenoidal detector optimized for the asymmetric-energy beams at PEP-II and is described in [12]. We summarize briefly the components that are crucial to this analysis. Charged-particle tracking is provided by a five-layer silicon vertex tracker (SVT) and a 40-layer drift chamber (DCH). In addition to providing precise spatial hits for tracking, the SVT and DCH also measure the specific ionization (dE/dx), which is used for particle identification of low-momentum charged particles. At higher momenta ($p > 0.7$ GeV/c) pions and kaons are identified by Cherenkov radiation detected in a ring-imaging device (DIRC). The typical separation between pions and kaons varies from 8σ at 2 GeV/c to 2.5σ at 4 GeV/c. The position and energy of neutral clusters (photons) are measured with an electromagnetic calorimeter (EMC) consisting of 6580 thallium-doped CsI crystals. These systems are mounted inside a 1.5-T solenoidal super-conducting magnet.

3 EVENT SELECTION

We reconstruct the decays $B^- \to \tilde{D}^0 K^{*-}$ with $\tilde{D}^0 \to K^0_S\pi^-\pi^+$, $K^{*-} \to K^0_S\pi^-$ and $K^0_S \to \pi^-\pi^+$. The K^0_S candidates are formed from oppositely charged pions with a reconstructed invariant mass within 9 MeV/c^2 of the nominal K^0_S mass [2]. The two pions are constrained to originate from the same point. The $\tilde{D}^0$ candidates are selected by combining mass constrained K^0_S candidates with two oppositely charged pions having an invariant mass within 12 MeV/c^2 of the nominal $\tilde{D}^0$ mass [2]. The $\tilde{D}^0$ candidates are mass and vertex constrained. The K^{*-} candidates are selected from combinations of a K^0_S with a negative charged pion with an invariant mass within 55 MeV/c^2 of the nominal K^{*-} mass [2]. The cosine of the angle between the direction transverse to the beam connecting the $\tilde{D}^0$ or K^{*-} and the K^0_S decay points (transverse flight direction), and the K^0_S transverse momentum vector is required to be larger than 0.99. Since the K^{*-} in $B^- \to \tilde{D}^0 K^{*-}$ is polarized, we require $|\cos\theta_H| \geq 0.35$, where θ_H is the angle in the K^{*-} rest frame between the daughter pion and the parent B momentum. The distribution of $\cos\theta_H$ is proportional to $\cos^2\theta_H$ for the $B^- \to \tilde{D}^0 K^{*-}$ signal and is roughly flat for the $e^+e^- \to q\bar{q}$ ($q = u, d, s, c$) continuum background. The B^- candidates are reconstructed by combining a $\tilde{D}^0$ candidate with a K^{*-} candidate. We select the B mesons by using the beam-energy substituted mass, $m_{\mathrm{ES}} = \sqrt{(E^{*2}_i/2 + \mathbf{p_i}\cdot\mathbf{p_B})^2/E^2_i - p^2_B}$,

and the energy difference $\Delta E = E_B^* - E_i^*/2$, where the subscripts i and B refer to the initial e^+e^- system and the B candidate, respectively, and the asterisk denotes the center-of-mass (CM) frame. The resolutions of $m_{\rm ES}$ and ΔE, evaluated on simulated signal events, are 2.6 MeV/c^2 and 11 MeV, respectively. We define a selection region through the requirement $|\Delta E| < 25$ MeV and $m_{\rm ES} > 5.2$ GeV/c^2. To suppress the background from continuum events we require $|\cos\theta_T| < 0.8$ where θ_T is defined as the angle between the thrust axis of the B candidate and that of the rest of the event. After all the cuts are applied the average number of candidates per event is 1.06. We select one B candidate per event by taking the one that has the minimum value of a χ^2 built with the $\tilde{D}^0$ and K^* masses, resolutions and intrinsic width for the case of the K^*. The $B^- \to \tilde{D}^0 K^{*-}$ reconstruction efficiency is $11.1 \pm 0.5\%$ for simulated events. The reconstruction purity in the signal region $m_{\rm ES} > 5.272$ GeV/c^2 is estimated to be 46%. Figure 1 shows the $m_{\rm ES}$ distribution after all the selection criteria are applied.

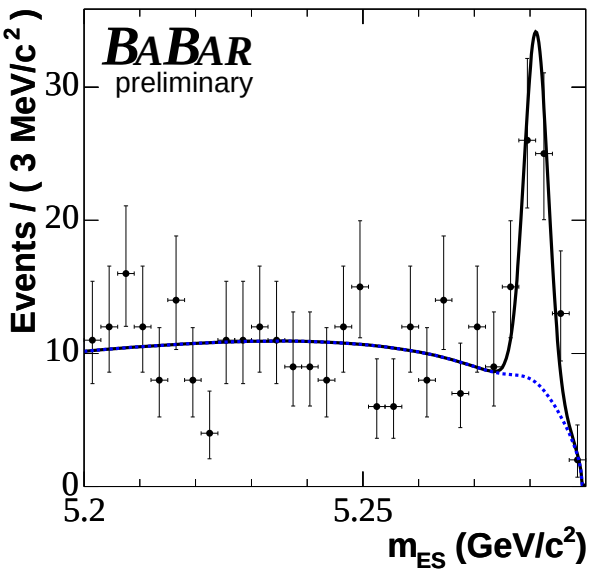

Figure 1: $B^- \to \tilde{D}^0 K^{*-}$ $m_{\rm ES}$ distribution after all selection criteria are applied. The curves represent the fit projections for signal plus background (solid) and background (dotted).

4 THE $D^0 \to K^0_S\pi^-\pi^+$ DECAY MODEL

The $D^0 \to K^0_S\pi^-\pi^+$ decay amplitude $\mathcal{A}_D(m_-^2, m_+^2)$ is determined from an unbinned maximum-likelihood Dalitz fit to the Dalitz plot distribution of a high-purity (97%) sample of 81496 $D^{*+} \to D^0\pi^+$ decays reconstructed in 91.5 fb^{-1} of data, shown in Fig. 2(a). We use two different models to describe $\mathcal{A}_D(m_-^2, m_+^2)$.

The first (Breit-Wigner) model is the same as used for our previously reported measurement of γ on $B^- \to \tilde{D}^{(*)0}K^-$, $\tilde{D}^0 \to K^0_S\pi^-\pi^+$ decays [5]. Here, the decay amplitude is expressed as a sum of two-body decay-matrix elements (subscript r) and a non-resonant (subscript NR) contribution,

$$\mathcal{A}_D(m_-^2, m_+^2) = \Sigma_r a_r e^{i\phi_r} \mathcal{A}_r(m_-^2, m_+^2) + a_{\rm NR} e^{i\phi_{\rm NR}} \ ,$$

where each term is parameterized with an amplitude a_r and a phase ϕ_r. The function $\mathcal{A}_r(m_-^2, m_+^2)$ is the Lorentz-invariant expression for the matrix element of a D^0 meson decaying into $K_S^0\pi^-\pi^+$ through an intermediate resonance r, parameterized as a function of position in the Dalitz plane. For $r = \rho(770)$ and $\rho(1450)$ we use the functional form suggested in Ref. [13], while the remaining resonances are parameterized by a spin-dependent relativistic Breit-Wigner distribution [2]. The model consists of 13 resonances leading to 16 two-body decay amplitudes and phases (see Table I in Ref. [5]), plus the non-resonant contribution, and accounts for efficiency variations across the Dalitz plane and the small background contribution (with uniform Dalitz shape). All the resonances considered in this model are well established except for the two scalar $\pi\pi$ resonances, σ and σ', whose masses and widths are obtained from our sample. The σ and σ' resonances are introduced in order to obtain a better fit to the data, but we consider in the evaluation of the systematic errors the possibility that they do not actually exist. We estimate the goodness of fit through a two-dimensional χ^2 test and obtain $\chi^2 = 3824$ for $3054 - 32$ degrees of freedom. This model is the one used as nominal in this analysis.

The second ($\pi\pi$ S-wave K-matrix) model uses the K-matrix formalism [10, 11] to parameterize the S-wave component of the $\pi\pi$ system in $D^0 \to K_S^0\pi^-\pi^+$. The K-matrix approach can be applied to the case of resonance production in multi-body decays when the two-body system in the final state is isolated, and the two particles do not interact simultaneously with the rest of the final state in the production process. In addition, it provides a direct way of imposing the unitarity constraint that is not guaranteed in the case of the Breit-Wigner model. Therefore, the K-matrix method is suited to the study of broad and overlapping resonances in multi-channel decays, solving the main limitation of the Breit-Wigner model to parameterize the $\pi\pi$ S-wave states in $D^0 \to K_S^0\pi^-\pi^+$ [14], and avoiding the need to introduce the two σ scalars.

The Dalitz amplitude $\mathcal{A}_D(m_-^2, m_+^2)$ is written in this case as a sum of two-body decay matrix elements for the spin-1, spin-2 and $K\pi$ spin-0 resonances (as in the Breit-Wigner model), and the $\pi\pi$ spin-0 piece denoted as F_1 is written in terms of the K-matrix. We have

$$\mathcal{A}_D(m_-^2, m_+^2) = F_1(s) + \Sigma_{r\neq\pi\pi\,\mathrm{S-wave}} a_r e^{i\phi_r} \mathcal{A}_r(m_-^2, m_+^2) \ , \tag{3}$$

where $F_1(s)$ is the contribution of $\pi\pi$ S-wave states,

$$F_1(s) = \sum_j \left[I - iK(s)\rho(s)\right]^{-1}_{1j} P_j(s) \ . \tag{4}$$

Here, s is the squared mass of the $\pi\pi$ system ($m^2_{\pi^+\pi^-}$), I is the identity matrix, K is the matrix describing the S-wave scattering process, ρ is the phase-space matrix, and P is the initial production vector [11],

$$P_j(s) = \sum_\alpha \frac{\beta_\alpha g_j^\alpha}{m_\alpha^2 - s} + f_{1j}^{\mathrm{prod}} \frac{1 - s_0^{\mathrm{scatt}}}{s - s_0^{\mathrm{scatt}}} \ . \tag{5}$$

The index j represents the j^{th} channel ($1 = \pi\pi$, $2 = K\overline{K}$, $3 =$multi-meson[5], $4 = \eta\eta$, $5 = \eta\eta'$ [15]). The K-matrix parameters are obtained from Ref. [15] from a global fit of the available $\pi\pi$ scattering data from threshold up to $1900\,\mathrm{MeV}/c^2$. The K-matrix parameterization is

$$K_{ij}(s) = \left\{ \sum_\alpha \frac{g_i^\alpha g_j^\alpha}{m_\alpha^2 - s} + f_{ij}^{\mathrm{scatt}} \frac{1.0 - s_0^{\mathrm{scatt}}}{s - s_0^{\mathrm{scatt}}} \right\} \frac{(1 - s_{A0})}{(s - s_{A0})} (s - s_A m_\pi^2/2), \tag{6}$$

[5]Multi-meson channel refers to a final state with four pions.

Table 1: K-matrix parameters as obtained from Refs. [15, 18]. Pole masses (m_α) and coupling constants (g_i^α) are given in GeV/c^2, $s_0^{\rm scatt}$ and s_{A0} are in GeV$^2/c^4$.

m_α	$g^\alpha_{\pi^+\pi^-}$	$g^\alpha_{K\overline{K}}$	$g^\alpha_{4\pi}$	$g^\alpha_{\eta\eta}$	$g^\alpha_{\eta\eta'}$
0.651	0.229	−0.554	0.000	−0.399	−0.346
1.204	0.941	0.551	0.000	0.391	0.315
1.558	0.369	0.239	0.556	0.183	0.187
1.210	0.337	0.409	0.857	0.199	−0.010
1.822	0.182	−0.176	−0.797	−0.004	0.224

$f_{11}^{\rm scatt}$	$f_{12}^{\rm scatt}$	$f_{13}^{\rm scatt}$	$f_{14}^{\rm scatt}$	$f_{15}^{\rm scatt}$
0.234	0.150	−0.206	0.328	0.354

$s_0^{\rm scatt}$	s_{A0}	s_A
−3.926	−0.15	1

where g_i^α is the coupling constant of the K-matrix pole m_α to the $i^{\rm th}$ channel. The parameters $f_{ij}^{\rm scatt}$ and $s_0^{\rm scatt}$ describe the slowly-varying part of the K-matrix element. The Adler zero factor $(1-s_{A0})(s-s_A m_\pi^2/2)/(s-s_{A0})$ [16] suppresses false kinematical singularity at $s=0$ in the physical region near the $\pi\pi$ threshold [17]. Note that the production vector has the same poles as the K-matrix, otherwise the F_1 vector would vanish (diverge) at the K-matrix (P-vector) poles. The parameter values used in this analysis are listed in Table 1 [18]. The parameters $f_{ij}^{\rm scatt}$, for $i \neq 1$, are all set to zero since they are not related to the $\pi\pi$ scattering process.

The phase space matrix is diagonal, $\rho_{ij}(s) = \delta_{ij}\rho_i(s)$, where

$$\rho_i(s) = \sqrt{1 - \frac{(m_{1i}+m_{2i})^2}{s}}\ , \tag{7}$$

with m_{1i} (m_{2i}) denoting the mass of the first (second) final state particle of the i^{th} channel. The normalization is such that $\rho_i \to 1$ as $s \to \infty$. We use an analytic continuation of the ρ_i functions below threshold. The expression of the multi-meson state phase space is written as [15]

$$\rho_3(s) \ = \left\{ \begin{array}{ll} \rho_{31} & s < 1\ \ {\rm GeV}^2 \\ \rho_{32} & s > 1\ \ {\rm GeV}^2 \end{array} \right\}, \tag{8}$$

where

$$\begin{aligned} \rho_{31}(s) &= \rho_0 \int\int \frac{ds_1}{\pi}\frac{ds_2}{\pi} \frac{M^2\Gamma(s_1)\Gamma(s_2)\sqrt{(s+s_1-s_2)^2-4ss_1}}{s[(M^2-s_1)^2+M^2\Gamma^2(s_1)]\,[(M^2-s_2)^2+M^2\Gamma^2(s_2)]}, \\ \rho_{32}(s) &= \frac{s-16m_\pi^2}{s}\ . \end{aligned} \tag{9}$$

Here s_1 and s_2 are the squared invariant mass of the two dipion systems, M is the ρ meson mass, and $\Gamma(s)$ is the energy-dependent width. The factor ρ_0 provides the continuity of $\rho_3(s)$ at $s = 1$ GeV^2. Energy conservation in the dipion system must be satisfied when calculating the integral. This complicated expression reveals the fact that the ρ meson has an intrinsic width. If

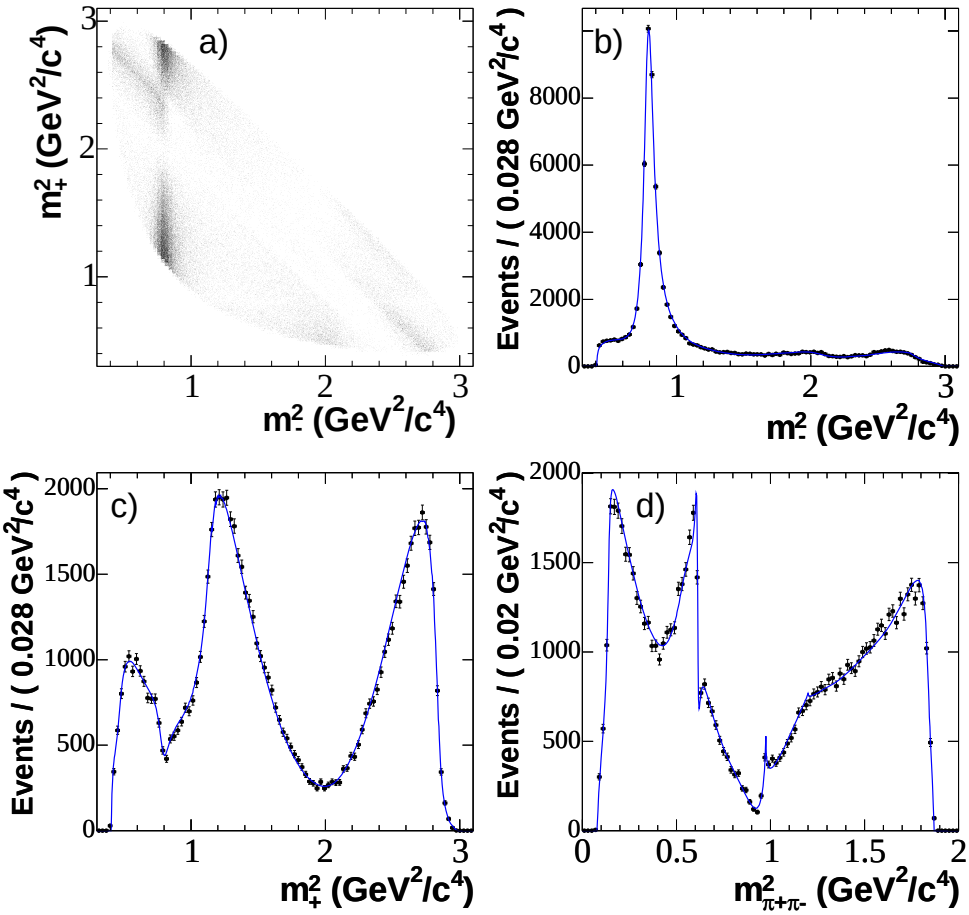

Figure 2: (a) The $D^0 \to K^0_S\pi^-\pi^+$ Dalitz distribution from $D^{*+} \to D^0\pi^+$ events, and projections on (b) m^2_-, (c) m^2_+, and (d) $m^2_{\pi^+\pi^-}$. $\overline{D}^0 \to K^0_S\pi^+\pi^-$ from $D^{*-} \to \overline{D}^0\pi^-$ events are also included. The curves are the $\pi\pi$ S-wave K-matrix model fit projections.

one sets $\Gamma(s) = \delta(s)$, where δ is the Dirac δ function, the usual two-body phase space factor is obtained.

Table 2 summarizes the values of the P-vector free parameters β_α and $f_{11}^{\rm prod}$ (we are describing only $\pi\pi$ channel), together with the spin-1, spin-2, and $K\pi$ spin-0 amplitudes as in the Breit-Wigner model. The third and fifth poles are not included since they are far beyond our $\pi\pi$ kinematic range. Figures 2(b,c,d) show the fit projections overlaid with the data distributions. There is no overall improvement in the two-dimensional χ^2 test compared to the Breit-Wigner model [5] since it is dominated by the P-wave components, which are identical between the two models. The total fit fraction is slightly changed from 1.24 to 1.16. Nevertheless, it should be emphasized that the main advantage of using a K-matrix parameterization rather than a sum of two-body amplitudes to describe the $\pi\pi$ S-wave is that it provides a more adequate description of the complex dynamics in the presence of overlapping and many channel resonances.

Table 2: Complex amplitudes $a_r e^{i\phi_r}$ and fit fractions of the different components ($K^0_S\pi^-$ and $K^0_S\pi^+$ resonances, and $\pi^+\pi^-$ poles) obtained from the fit of the $D^0 \to K^0_S\pi^-\pi^+$ Dalitz distribution from $D^{*+} \to D^0\pi^+$ events. Errors are statistical only. Masses and widths of all resonances are taken from [2], while the pole masses and scattering data are from [15, 18]. The fit fraction is defined for the resonance terms ($\pi\pi$ S-wave term) as the integral of $a_r^2|\mathcal{A}_r(m_-^2, m_+^2)|^2$ ($|F_1(s)|^2$) over the Dalitz plane divided by the integral of $|\mathcal{A}_D(m_-^2, m_+^2)|^2$. The sum of fit fractions is 1.16.

Component	$\mathrm{Re}\{a_r e^{i\phi_r}\}$	$\mathrm{Im}\{a_r e^{i\phi_r}\}$	Fit fraction (%)
$K^*(892)^-$	-1.159 ± 0.022	1.361 ± 0.020	58.9
$K^*_0(1430)^-$	2.482 ± 0.075	-0.653 ± 0.073	9.1
$K^*_2(1430)^-$	0.852 ± 0.042	-0.729 ± 0.051	3.1
$K^*(1410)^-$	-0.402 ± 0.076	0.050 ± 0.072	0.2
$K^*(1680)^-$	-1.00 ± 0.29	1.69 ± 0.28	1.4
$K^*(892)^+$	0.133 ± 0.008	-0.132 ± 0.007	0.7
$K^*_0(1430)^+$	0.375 ± 0.060	-0.143 ± 0.066	0.2
$K^*_2(1430)^+$	0.088 ± 0.037	-0.057 ± 0.038	0.0
$\rho(770)$	1 (fixed)	0 (fixed)	22.3
$\omega(782)$	-0.0182 ± 0.0019	0.0367 ± 0.0014	0.6
$f_2(1270)$	0.787 ± 0.039	-0.397 ± 0.049	2.7
$\rho(1450)$	0.405 ± 0.079	-0.458 ± 0.116	0.3
β_1	-3.78 ± 0.13	1.23 ± 0.16	–
β_2	9.55 ± 0.20	3.43 ± 0.40	–
β_4	12.97 ± 0.67	1.27 ± 0.66	–
f_{11}^{prod}	-10.22 ± 0.32	-6.35 ± 0.39	–
sum of $\pi^+\pi^-$ S-wave			16.2

5 CP ANALYSIS

We perform an unbinned extended maximum-likelihood fit to the $B^- \to \tilde{D}^0 K^{*-}$ sample to extract the *CP*-violating parameters $x_{s\mp}$, $y_{s\mp}$, and r_s^2 along with the signal and background yields. The $x_{s\pm}$ and $y_{s\pm}$ variables are more suitable fit parameters than κr_s, δ_s and γ because they are better behaved near the origin, especially in low-statistics samples. The fit uses m_{ES} and the same Fisher discriminant $\mathcal{F}$ as used in [5] to distinguish events from $B\overline{B}$ production and continuum background. The Fisher is a linear combination of four topological variables: $L_0 = \sum_i p_i^*$, $L_2 = \sum_i p_i^* |\cos\theta_i^*|^2$, and the absolute values of the cosine of the CM polar angles of the B candidate momentum and thrust direction. Here, p_i^* and θ_i^* are the CM momentum and the angle with respect to the B candidate thrust axis of the remaining tracks and clusters in the event. The likelihood for candidate j is obtained by summing the product of the event yield N_c, the probability density functions (PDF's) for the kinematic and event shape variables $\mathcal{P}_c$, and the Dalitz distributions $\mathcal{P}_c^{\mathrm{Dalitz}}$, over the signal and background components c. The overall likelihood function is

$$\mathcal{L} = \exp\left(-\sum_c N_c\right) \prod_j \sum_c N_c \mathcal{P}_c(\vec{\xi}_j) \mathcal{P}_c^{\mathrm{Dalitz}}(\vec{\eta}_j) \ ,$$

where $\vec{\xi}_j = \{m_{\rm ES}, \mathcal{F}\}_j$, $\vec{\eta}_j = (m_-^2, m_+^2)_j$, and $\mathcal{P}_c(\vec{\xi}) = \mathcal{P}_c(m_{\rm ES})\mathcal{P}_c(\mathcal{F})$. The components in the fit are signal, continuum background, and $B\overline{B}$ background. For signal events, $\mathcal{P}_c^{\rm Dalitz}(\vec{\eta})$ is given by $\Gamma_\mp(\vec{\eta})$ corrected by the efficiency variations, where $\Gamma_\mp(\vec{\eta})$ is given by Eq. (2). The $m_{\rm ES}$ ($\mathcal{F}$) distribution for signal events is described by a Gaussian (double-Gaussian) function distribution whose parameters are determined from a fit to the same $B^- \to D^0\pi^-$ high-statistics control sample as in our previous analysis [5].

5.1 Background composition

The event yields N_c for signal, continuum, and $B\overline{B}$ components are, respectively, 42 ± 8, 251 ± 24, and 45 ± 21, in agreement with our expectation from simulation and measured branching ratios. The dominant background contribution is from the random combination of a real or fake D^0 meson with a charged track and a K_S^0 in continuum events or other $B\overline{B}$ decays. The continuum background in the $m_{\rm ES}$ distribution is described by a threshold function [19] whose free parameter ζ is determined from the $B^- \to D^0\pi^-$ control sample. The Fisher PDF for continuum background is determined using $B^- \to D^0\pi^-$ events from the $m_{\rm ES}$ sideband region. The shape of the background $m_{\rm ES}$ distribution in generic $B\overline{B}$ decays is taken from simulation and uses a threshold function to describe the combinatorial component plus a Gaussian distribution to parameterize the peaking contribution arising from events with a misreconstructed pion and having a topology similar to that of signal events. The Gaussian component has a width of 3.8 ± 1.4 GeV/c^2 and its fraction with respect to the total $B\overline{B}$ background is 0.13 ± 0.03. The Fisher PDF and the mean of the $m_{\rm ES}$ Gaussian for $B\overline{B}$ events are assumed to be the same as that for the signal.

An important class of background events arises from continuum and $B\overline{B}$ background events where a real D^0 is produced back-to-back with a K^* in the CM. Depending on the flavor-charge correlation this background can mimic either the $b \to c$ or the $b \to u$ signal component. In the likelihood function we take this effect into account with two parameters, the fraction f_{D^0} of background events with a real D^0 and the parameter R, the fraction of background events with a real D^0 associated with an oppositely flavored kaon (same charge correlation as the $b \to u$ signal component). These fractions have been evaluated separately from continuum and generic $B\overline{B}$ simulated events, and are found to be $f_{D^0}^{q\overline{q}} = 0.21 \pm 0.02$, $f_{D^0}^{B\overline{B}} = 0.18 \pm 0.02$, $R^{q\overline{q}} = 0.51 \pm 0.06$ and $R^{B\overline{B}} = 0.67 \pm 0.06$. In addition, to check the reliability of these estimates, the fraction f_{D^0} for all background (continuum and $B\overline{B}$) events has been evaluated from data using events satisfying $m_{\rm ES} < 5.272$ GeV/c^2 after removing the requirement on the D^0 mass cut. The measured value of 0.20 ± 0.06 is consistent with the continuum and $B\overline{B}$ fractions obtained from simulated events. The shapes of the Dalitz plot distributions are parameterized by a third-order polynomial in (m_-^2, m_+^2) for the combinatorial component (fake D^0) and as signal D^0 or $\overline{D}^0$ shapes for real neutral D mesons. The parameters of the polynomials are extracted from off-resonance data and sidebands for the continuum component, while we use the simulation for $B\overline{B}$.

A potentially dangerous background originates from signal $B^- \to \tilde{D}^0 K^{*-}$ where the $\tilde{D}^0$ meson is combined with a random K^* or pion from the other B meson having the opposite charge. Using simulated events the fraction of these wrong sign signal events is found to be $(0.43 \pm 0.05)\%$, and therefore this contribution has been neglected.

5.2 *CP* parameters

The Dalitz plot distributions for the $\tilde{D}^0 \to K_S^0\pi^-\pi^+$ decay from $B^- \to \tilde{D}^0 K^{*-}$ for events with $m_{\rm ES} > 5.272$ GeV/c^2 are shown in Fig. 3. The distributions for B^- and B^+ candidates are shown

Table 3: *CP*-violating parameters $(x_{s\pm}, y_{s\pm})$ obtained from the *CP* fit to the $B^- \to \tilde{D}^0 K^{*-}$ sample. The first error is statistical, the second is the experimental systematic uncertainty and the third reflects the Dalitz model uncertainty.

CP parameter	Result
$x_{s-} \equiv \kappa r_s \cos(\delta_s - \gamma)$	$-0.20 \pm 0.20 \pm 0.11 \pm 0.03$
$y_{s-} \equiv \kappa r_s \sin(\delta_s - \gamma)$	$0.26 \pm 0.30 \pm 0.16 \pm 0.03$
$x_{s+} \equiv \kappa r_s \cos(\delta_s + \gamma)$	$-0.07 \pm 0.23 \pm 0.13 \pm 0.03$
$y_{s+} \equiv \kappa r_s \sin(\delta_s + \gamma)$	$-0.01 \pm 0.32 \pm 0.18 \pm 0.05$

separately. The results for the *CP*-violating parameters $x_{s\pm}$ and $y_{s\pm}$ obtained by fitting those distributions are summarized in Table 3. From the same fit we obtain for r_s^2 the value 0.05 ± 0.11 (statistical error only). The only relevant statistical correlations involving the *CP* parameters are for the pairs (x_{s-}, y_{s-}) and (x_{s+}, y_{s+}), which amount to -10.1% and 2.2%, respectively. The statistical correlation of r_s^2 with x_{s-}, y_{s-}, x_{s+}, and y_{s+} are -22.6%, 3.7%, -25.1%, and 22.0%, respectively. The Dalitz distribution projections on m_-^2, m_+^2 and $m_{\pi^+\pi^-}^2$ for events satisfying $m_{\rm ES} > 5.272$ GeV/c^2 are compared to the projection of the fit in Fig. 4, separately for B^- and B^+ events. Figure 5 shows the two-dimensional one- (dark) and two- (light) standard deviation regions (statistical only) in the (x_s, y_s) plane, corresponding to 39.3% and 86.5% probability content, separately for $B^- \to \tilde{D}^0 K^{*-}$ and $B^+ \to \tilde{D}^0 K^{*+}$. The separation d between the B^- and B^+ regions in these planes is proportional to the amount of direct *CP* violation, $d = 2\kappa r_s |\sin\gamma|$.

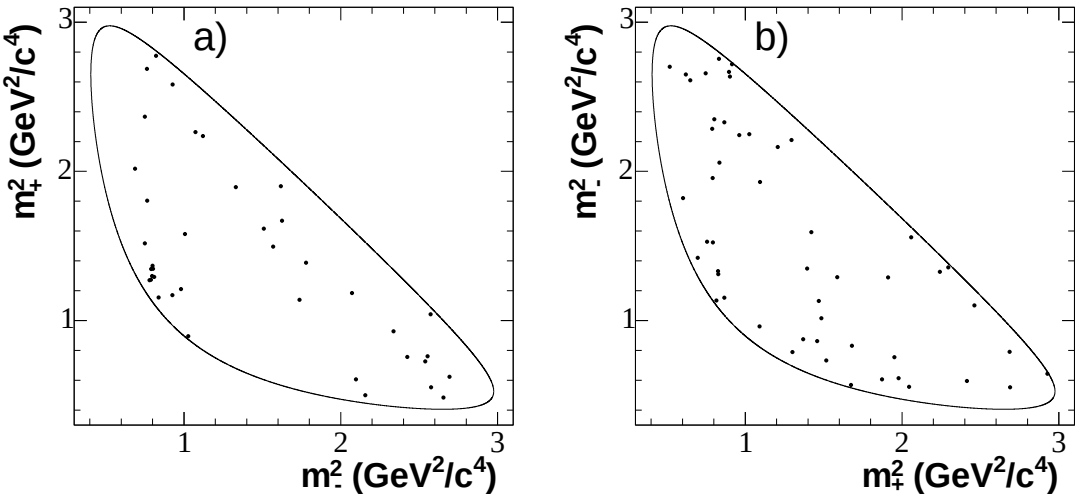

Figure 3: The $\tilde{D}^0 \to K_S^0\pi^-\pi^+$ Dalitz distributions from (a) $B^- \to \tilde{D}^0 K^{*-}$ and (b) $B^+ \to \tilde{D}^0 K^{*+}$ events with $m_{\rm ES} > 5.272$ GeV/c^2.

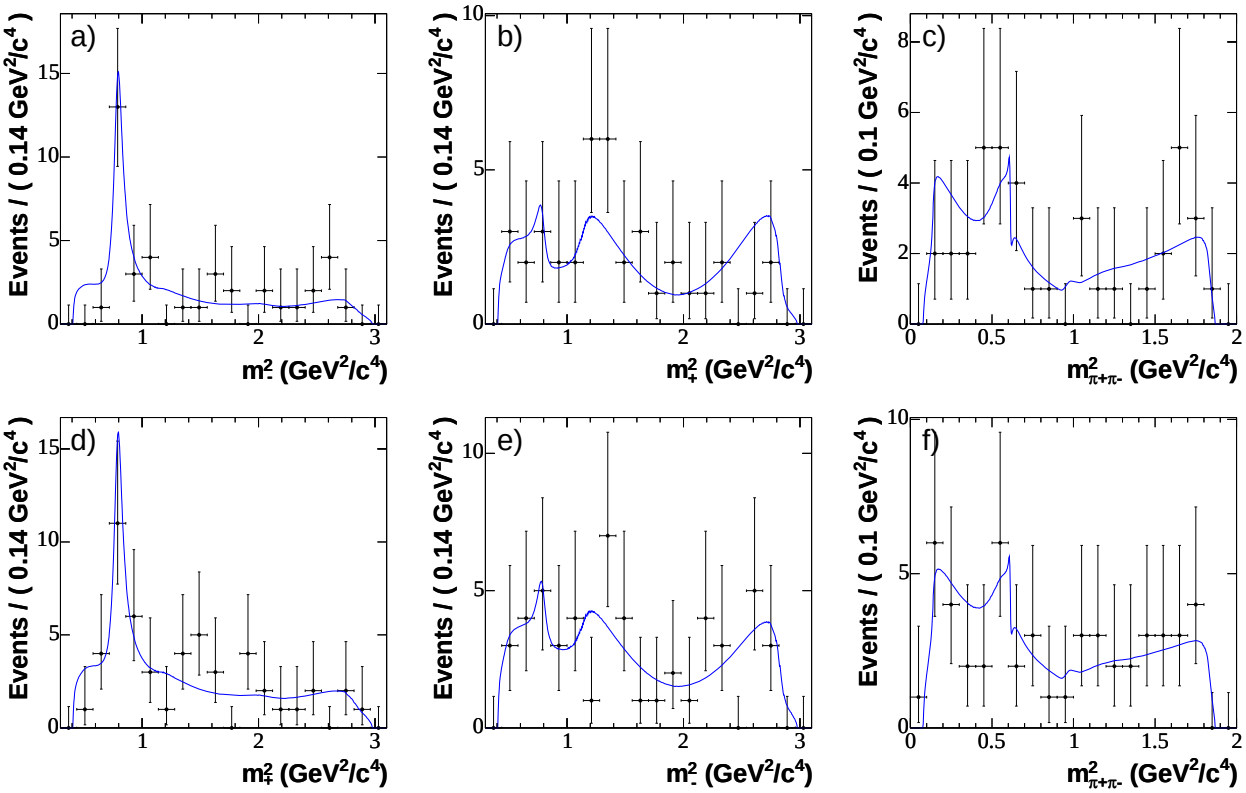

Figure 4: Projections of the Dalitz distributions on m_-^2, m_+^2 and $m_{\pi^+\pi^-}^2$ from a)b)c) $B^- \to \tilde{D}^0 K^{*-}$ and d)e)f) $B^+ \to \tilde{D}^0 K^{*+}$ events with $m_{\rm ES} > 5.272$ GeV/c^2. The projections of the fit result are superimposed.

5.3 Experimental systematic errors

Table 4 summarizes the break down of the experimental systematic uncertainties. These include the errors on the $m_{\rm ES}$ and $\mathcal{F}$ PDF parameters for signal and background, the uncertainties in the knowledge of the Dalitz distribution of background events, the efficiency variations across the Dalitz plane, and the uncertainty in the fraction of events with a real D^0 produced in a back-to-back configuration with a negatively-charged kaon. Less significant systematic uncertainties originate from the imprecise knowledge of the fraction of real D^0's, the invariant mass resolution (negligible), tracking efficiency, and the statistical errors in the Dalitz amplitudes and phases from the fit to the tagged D^0 sample. We quote as systematic uncertainty, for each effect, the maximum of the difference between the bias and square root of the quadratic difference of the statistical error between the nominal fit result and the one corresponding to the effect under consideration. These systematic uncertainties will be reduced with a larger data and simulated samples and are not expected to limit the eventual sensitivity of the analysis.

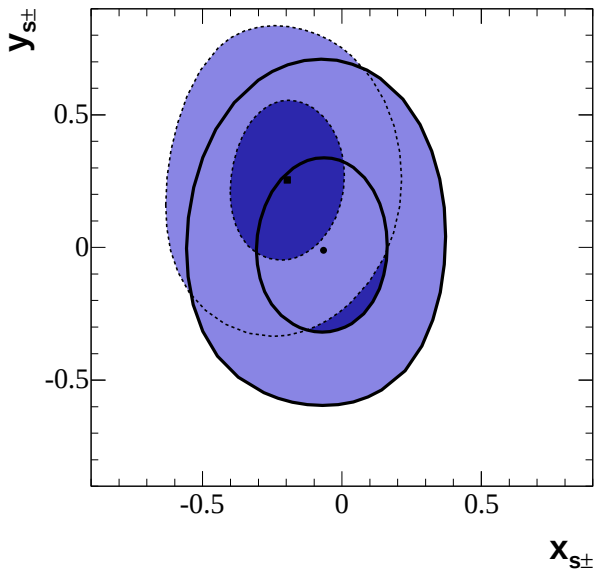

Figure 5: Two-dimensional one- (dark) and two- (light) standard deviation regions (statistical only) in the (x_s, y_s) plane, corresponding to 39.3% and 86.5% probability content, separately for $B^- \to \tilde{D}^0 K^{*-}$ (thick and solid) and $B^+ \to \tilde{D}^0 K^{*+}$ (thin and dotted). The confidence regions for B^+ are superimposed over those for B^-.

5.4 $\tilde{D}^0 \to K^0_S \pi^- \pi^+$ Dalitz model systematic uncertainty

The largest single contribution to the systematic uncertainties in the *CP* parameters comes from the choice of the Dalitz model used to describe the $D^0 \to K^0_S \pi^- \pi^+$ decay amplitude $\mathcal{A}_D$. We use the same procedure as in our previous measurement [5] to evaluate this uncertainty. We first generate large samples of pseudo-experiments using the nominal (Breit-Wigner) model. Since the effect on the *CP* parameters depends on their generated values, for each pseudo-experiment we randomly generate the truth values of the Cartesian *CP* parameters according to their measured central values and statistical errors. We then compare experiment by experiment the values of the $x_{s\pm}$ and $y_{s\pm}$ obtained from fits using the nominal model and a set of alternative models. We find that models resulting by removing different combinations of higher K^* and ρ resonances (with low fit fractions), or changing the functional form of the resonance shapes, has little effect on the total χ^2 of the fit, or on the values of the *CP* parameters (at most 1° for γ and 0.002 for κr_s). As an extreme we consider a model without the σ_1 and/or σ_2 scalar resonances, or the CLEO Breit-Wigner model [9]. Fits to these models result in a significantly larger χ^2 than that of the nominal model, but the effect on the *CP* parameters are still small, as indicated in Table 4. These uncertainties translate to κr_s, γ and δ_s as 0.05, 9°, and 11°, respectively [6]. For $B^- \to \tilde{D}^{(*)0} K^-$ decays, the same procedure to propagate the uncertainties on $r_B^{(*)}$, γ, and $\delta_B^{(*)}$ gives 0.027(0.027), 11°, and 14°(13°), respectively.

As an additional cross-check of the fact that models without the σ scalars are in fact an extreme

[6] The Dalitz model uncertainties on κr_s, γ and δ_s are obtained by repeating the fits to the same high statistics pseudo-experiments but now fitting directly to these *CP* parameters. This method accounts for the systematic correlations among the Cartesian *CP*-violating parameters.

Table 4: Summary of the non-negligible contributions to the systematic error on the *CP* parameters $x_{s\pm}$ and $y_{s\pm}$.

Source	x_{s-}	y_{s-}	x_{s+}	y_{s+}
$m_{\rm ES}$, $\mathcal{F}$ shapes	0.08	0.12	0.10	0.12
Background Dalitz shape	0.04	0.09	0.04	0.09
Efficiency in the Dalitz plot	0.06	0.04	0.07	0.09
Right sign $\tilde{D}^0$ fractions ($R^{q\overline{q}}$, $R^{B\overline{B}}$)	0.03	0.04	0.03	0.05
Real $\tilde{D}^0$ fractions ($f_{D^0}^{q\overline{q}}$, $f_{D^0}^{B\overline{B}}$)	0.03	0.03	0.03	0.04
Tracking efficiency	0.01	0.01	0.01	0.01
Dalitz amplitudes and phases	0.01	0.01	0.01	0.01
Total experimental	0.11	0.16	0.13	0.18
Dalitz model (Breit-Wigner model without σ scalars)	0.03	0.03	0.03	0.05
Dalitz model ($\pi\pi$ S-wave K-matrix model)	0.01	0.01	0.01	0.01

case, we repeated the above procedure using as alternative model the $\pi\pi$ S-wave K-matrix model described in Sec. 4 instead of the CLEO Breit-Wigner model (the latter used to quote the Dalitz model systematic uncertainty, as described before). The effect on the Cartesian *CP* parameters is more than three times smaller, as shown in Table 4. These uncertainties translate to κr_s, γ and δ_s as 0.015, 3°, and 2°, respectively. For $B^- \to \tilde{D}^{(*)0}K^-$ decays, the scaling of the effect on the Cartesian *CP* parameters is similar to $B^- \to DK^{*-}$. In terms of $r_B^{(*)}$, γ, and $\delta_B^{(*)}$ the variation is 0.004(0.003), 2°, and 2°(2°), respectively.

6 INTERPRETATION AND RESULTS

A frequentist (Neyman) analysis [2] has been adopted to interpret the constraints on $\mathbf{z}_\pm \equiv (x_{s\pm}, y_{s\pm})$ in terms of $\mathbf{p} \equiv (\kappa r_s, \delta_s, \gamma)$. We construct an analytical parameterization of the four-dimensional probability density function $\mathcal{P}$ of $\mathbf{z}_\pm$ as a function of $\mathbf{p}$,

$$\frac{d^4\mathcal{P}}{d^2\mathbf{z}_+ d^2\mathbf{z}_-}(\mathbf{z}_+, \mathbf{z}_-|\mathbf{p}) \;=\; \frac{d^2\mathcal{P}}{d^2\mathbf{z}_+}(\mathbf{z}_+|\mathbf{p})\frac{d^2\mathcal{P}}{d^2\mathbf{z}_-}(\mathbf{z}_-|\mathbf{p}) \;, \tag{10}$$

where

$$\frac{d^2\mathcal{P}}{d^2\mathbf{z}_\pm}(\mathbf{z}_\pm|\mathbf{p}) \;=\; G_2\left[\mathbf{z}_\pm; \kappa r_s\cos(\delta_s \pm \gamma), \kappa r_s \sin(\delta_s \pm \gamma), \sigma_{x_{s\pm}}, \sigma_{y_{s\pm}}, \rho_{s\pm}\right] \tag{11}$$

is a two-dimensional Gaussian distribution [20]. Here, $\rho_{s\pm}$ represents the correlation between $x_{s\pm}$ and $y_{s\pm}$. For a given $\mathbf{p}$, the three-dimensional confidence level is estimated as $\mathcal{C}(\mathbf{p}) = 1 - \alpha(\mathbf{p})$, where $\alpha(\mathbf{p})$ is calculated by integrating Eq. (10) over a domain defined by all points in the four-dimensional fit parameter space closer (larger PDF) to $\mathbf{p}$ than the fitted data values,

$$\frac{d^4\mathcal{P}}{d^2\mathbf{z}_+ d^2\mathbf{z}_-}(\mathbf{z}_+, \mathbf{z}_-|\mathbf{p}) \geq \frac{d^4\mathcal{P}}{d^2\mathbf{z}_+ d^2\mathbf{z}_-}(\mathbf{z}_+^{\rm data}, \mathbf{z}_-^{\rm data}|\mathbf{p}) \;. \tag{12}$$

The one (two) standard deviation region of the *CP* parameters is defined as the set of $\mathbf{p}$ values (constructed from a large number of pseudo-experiments) for which $\alpha(\mathbf{p})$ is smaller than 19.88%

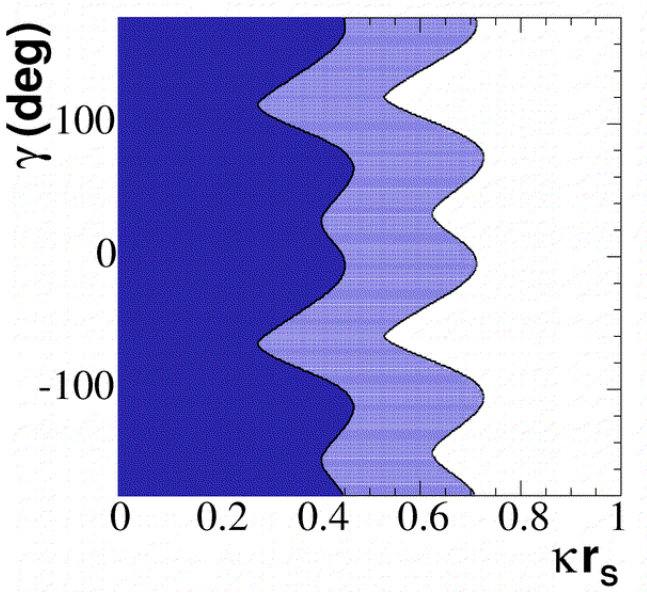

Figure 6: Two-dimensional projection onto the $\kappa r_s - \gamma$ plane of the three-dimensional one- (dark) and two- (light) standard deviation regions, including statistical and experimental systematic uncertainties, for $B^- \to \tilde{D}^0 K^{*-}$.

(73.85%). Figure 6 shows the constraints in the $\kappa r_s - \gamma$ plane as obtained by projecting the three-dimensional confidence regions, including statistical and experimental systematic uncertainties.

$B^- \to \tilde{D}^0 K^{*-}$ events can be used in combination with $B^- \to \tilde{D}^{(*)0} K^-$ [5] to improve the overall constraints on γ. The procedure used to combine the three B decay channels is identical to the one described above, but with increased number of dimensions. In this case, the dimension of the fit parameter space is twelve, $\mathbf{z}_\pm \equiv (x_\pm^{(*)}, y_\pm^{(*)}, x_{s\pm}, y_{s\pm})$. The *CP* parameter space has instead seven dimensions, $\mathbf{p} \equiv (r_B^{(*)}, \delta_B^{(*)}, \kappa r_s, \delta_s, \gamma)$. The one (two) standard deviation region of the *CP* parameters is defined as the set of $\mathbf{p}$ values for which $\alpha(\mathbf{p})$ is larger than 0.52% (22.02%). Figure 7 shows the two-dimensional projections onto the $r_B - \gamma$, $r_B^* - \gamma$, and $\kappa r_s - \gamma$ planes, including statistical and experimental systematic uncertainties. The figures show that this Dalitz analysis has a two-fold ambiguity. The combination if the three signal modes yields $\gamma = (67 \pm 28 \pm 13 \pm 11)^\circ$, where the first error is statistical, the second is the experimental systematic uncertainty and the third reflects the Dalitz model uncertainty. Of the two possible solutions we choose the one with $0 < \gamma < 180^\circ$. The contribution to the Dalitz model uncertainty due to the description of the $\pi\pi$ S-wave in $D^0 \to K_S^0 \pi^- \pi^+$ is 3°. From this combination, κr_s is constrained to be < 0.50 (0.75) at one (two) standard deviation level. It is worth noting that the value of κr_s depends on the selected phase space region of $B^- \to \tilde{D}^0 (K_S^0 \pi^-)$ events without introducing any bias on the extraction of γ.

The constraint on γ is consistent with that reported by the Belle Collaboration [6, 7]. However, the statistical error turns out to be larger than that of Belle because our data favors smaller values of $r_B^{(*)}$ and κr_s. Simulation studies confirm that the difference in statistical errors is consistent with the scaling expected from the different actual values.

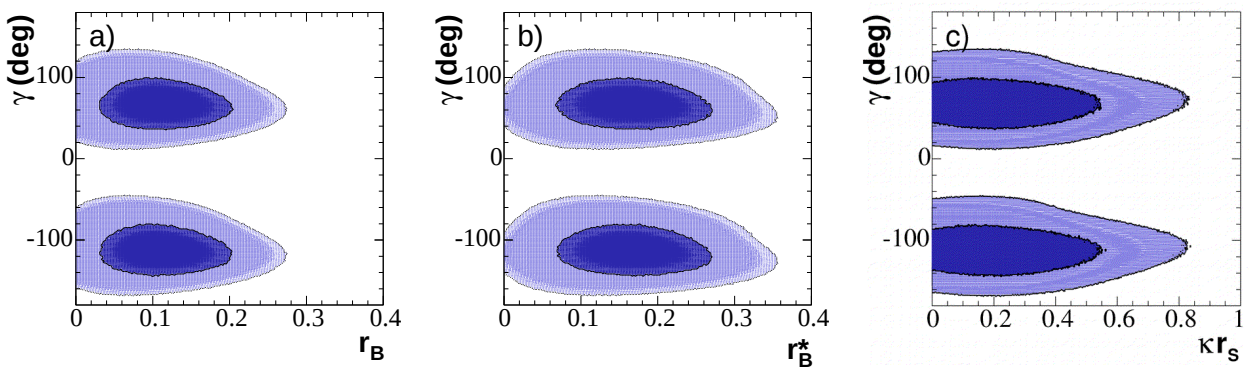

Figure 7: Two-dimensional projections onto the (a) $r_B - \gamma$, (b) $r_B^* - \gamma$, and (c) $\kappa r_s - \gamma$ planes of the seven-dimensional one- (dark) and two- (light) standard deviation regions, for the combination of $B^- \to \tilde{D}^{(*)0} K^-$ and $B^- \to \tilde{D}^0 K^{*-}$ modes.

7 ACKNOWLEDGMENTS

We are grateful for the extraordinary contributions of our PEP-II colleagues in achieving the excellent luminosity and machine conditions that have made this work possible. The success of this project also relies critically on the expertise and dedication of the computing organizations that support *BABAR*. The collaborating institutions wish to thank SLAC for its support and the kind hospitality extended to them. This work is supported by the US Department of Energy and National Science Foundation, the Natural Sciences and Engineering Research Council (Canada), Institute of High Energy Physics (China), the Commissariat à l'Energie Atomique and Institut National de Physique Nucléaire et de Physique des Particules (France), the Bundesministerium für Bildung und Forschung and Deutsche Forschungsgemeinschaft (Germany), the Istituto Nazionale di Fisica Nucleare (Italy), the Foundation for Fundamental Research on Matter (The Netherlands), the Research Council of Norway, the Ministry of Science and Technology of the Russian Federation, and the Particle Physics and Astronomy Research Council (United Kingdom). Individuals have received support from CONACyT (Mexico), the A. P. Sloan Foundation, the Research Corporation, and the Alexander von Humboldt Foundation.

References

[1] N. Cabibbo, Phys. Rev. Lett. **10**, 531 (1963); M. Kobayashi and T. Maskawa, Prog. Theor. Phys. **49**, 652 (1973).

[2] Particle Data Group, S. Eidelman *et al.*, Phys. Lett. B **592**, 1 (2004).

[3] M. Gronau and D. London, Phys. Lett. B **253**, 483 (1991); M. Gronau and D. Wyler, Phys. Lett. B **265**, 172 (1991); D. Atwood, I. Dunietz and A. Soni, Phys. Rev. Lett. **78**, 3257 (1997).

[4] A. Giri, Yu. Grossman, A. Soffer and J. Zupan, Phys. Rev. D **68**, 054018 (2003).

[5] *BABAR* Collaboration, B. Aubert *et al.*, hep-ex/0504039, Accepted by Phys. Rev. Lett. .

[6] Belle Collaboration, A. Poluektov *et al.*, Phys. Rev. D **70**, 072003 (2004); K. Abe *et al.*, hep-ex/0411049.

[7] Belle Collaboration, K. Abe *et al.*, hep-ex/0504013.

[8] M. Gronau, Phys. Lett. **B557**, 198 (2003).

[9] CLEO Collaboration, S. Kopp *et al.*, Phys. Rev. D **63**, 092001 (2001); CLEO Collaboration, H. Muramatsu *et al.*, Phys. Rev. Lett. **89**, 251802 (2002); Erratum-ibid: **90** 059901 (2003).

[10] E. P. Wigner, Phys. Rev. 70 (1946) 15; S. U. Chung *et al.*, Ann. Physik 4 (1995) 404.

[11] I. J. R. Aitchison, Nucl. Phys. **A189**, 417 (1972).

[12] *BABAR* Collaboration, B. Aubert *et al.*, Nucl. Instrum. Methods **A479**, 1-116 (2002).

[13] G.J. Gounaris and J.J. Sakurai, Phys. Rev. Lett. **21**, 244, (1968).

[14] Review on Scalar Mesons in Ref. [2].

[15] V. V. Anisovich and A. V. Sarantev, Eur. Phys. Jour. A **16**, 229 (2003).

[16] FOCUS Collaboration, J. M. Link *et al.*, Phys. Lett. B **585**, 200 (2004). One should note that there is a misprint of the $(1 - s_{A0})$ factor in the Adler zero expression.

[17] S. L. Adler, Phys. Rev. **137**, B1022 (1965).

[18] V. V. Anisovich and A. V. Sarantev, private communication.

[19] $\frac{dN}{dm_{ES}} = N \cdot m_{\rm ES} \cdot \sqrt{1-x^2} \cdot \exp\left(-\zeta \cdot (1-x^2)\right)$ where $x = 2m_{\rm ES}/\sqrt{s}$ and the parameter ζ is determined from a fit. ARGUS Collaboration, H. Albrecht *et al.*, Z. Phys. C **48**, 543 (1990).

[20] As given by Eq. (31.28) in Ref. [2].